# Configuring pnicogen rings in skutterudites for low phonon conductivity

Hang Chi,[1] Hyoungchul Kim,[2] John C. Thomas,[3] Xianli Su,[1,4] Stephen Stackhouse,[5] Massoud Kaviany,[2] Anton Van der Ven,[3] Xinfeng Tang,[4] and Ctirad Uher[1,*]

[1]*Department of Physics, University of Michigan, Ann Arbor, Michigan 48109, USA*

[2]*Department of Mechanical Engineering, University of Michigan, Ann Arbor, Michigan 48109, USA*

[3]*Department of Materials Science and Engineering, University of Michigan, Ann Arbor, Michigan 48109, USA*

[4]*State Key Laboratory of Advanced Technology for Materials Synthesis and Processing, Wuhan University of Technology, Wuhan 430070, China*

[5]*School of Earth and Environment, University of Leeds, Leeds LS2 9JT, United Kingdom*

(Received 24 June 2012; published 29 November 2012)

Dominant heat-carrying modes in skutterudites are associated with vibrations of the pnicogen rings. Apart from filling the structural cages with foreign species, disrupting the pnicogen ring structure by substitutional alloying should be an effective approach to reduce thermal conductivity. In this paper we explore alloying configurations of pnicogen rings (Sb rings in the case of $CoSb_3$) that yield particularly low values of the thermal conductivity. We find that IV-VI double substitution (replacing two Sb atoms with one atom each from the column IV and column VI elements to achieve an average charge of two Sb atoms) is a very effective approach. Our *ab initio* calculations, in combination with a cluster expansion, have allowed us to identify stable alloy configurations on the Sb rings. Subsequent molecular and lattice dynamics simulations on low energy configurations establish the range of atomic displacement parameters and values of the thermal conductivity. Theoretical results are in good agreement with our experimental thermal conductivity values. Combining both approaches of compensated double substitution and filling of structural cages should be an effective way of improving the thermoelectric figure of merit of skutterudites.

DOI: 10.1103/PhysRevB.86.195209 PACS number(s): 64.75.Qr, 61.66.Dk, 63.20.dh, 63.20.dk

## I. INTRODUCTION

Filling structural cages in the $CoSb_3$ skutterudite crystal has proved to be an effective way of lowering lattice thermal conductivity,[1,2] making filled skutterudites one of the best novel thermoelectric (TE) materials for mid-temperature power generation applications.[3–5] An alternative approach to lowering thermal conductivity is to distort the near-square pnicogen (Sb) atomic rings, which are a characteristic feature of the skutterudite structure, thereby reducing the $Im\bar{3}(T_h^5)$ skutterudite space-group symmetry.[6] Since vibration modes involving Sb rings dominate the spectrum of heat-conducting phonons,[7,8] distortions of the rings should be particularly effective in disrupting heat transport. Ring deformation is easily accomplished via substitution of another species for Sb, with a historic focus on the *n*-type dopant Te.[9] Unfortunately, Te has a rather low solubility in $CoSb_3$ ($\leqslant 5\%$) and only weakly affects thermal conductivity. A charge-compensated alloy can be obtained by substitution of IV-VI species (e.g., Sn-Te[10] or Ge-Te[11,12]), which has recently been shown to enhance Te solubility and, in the case of Ge-Te, imbalanced Ge/Te induces formation of finely dispersed Ge-Te-rich skutterudite nanodots in the Sb-rich matrix. The enhanced point-defect scattering and presence of nanoinclusions in these double-substituted skutterudites enabled them to attain a TE figure of merit ($ZT$) of 1.1, competitive with the best values for single-filled skutterudites. These exciting empirical findings reveal a compelling theoretical puzzle surrounding the role of pnicogen ring configuration in skutterudite heat transport.

In this paper, we present a comprehensive theoretical analysis of the physical importance of pnicogen ring configuration on the thermal conductivity of the double-substituted skutterudite $CoSb_{3-m-n}Ge_mTe_n$. We use *ab initio* calculations to determine phase stability within $CoSb_{3-m-n}Ge_mTe_n$ and predict a strong energetic preference for short-range order of Ge and Te on pnicogen rings. While phase separation is predicted for charge-balanced $CoSb_{3(1-x)}Ge_{1.5x}Te_{1.5x}$, we find that it is sufficiently suppressed in the presence of coherency strains to make a solid solution experimentally accessible. New single-phase skutterudite samples of $CoSb_{3(1-x)}Ge_{1.5x}Te_{1.5x}$ have been successfully synthesized using the traditional melt-quench-anneal technique followed by spark plasma sintering (SPS). We explore the effect of the predicted short-range order of Ge and Te on lattice thermal conductivity and phonon dispersion of $CoSb_{3(1-x)}Ge_{1.5x}Te_{1.5x}$ solid solutions from first principles. Our thermal transport measurements support the idea that configurational disorder of pnicogen rings is an effective mechanism to reduce thermal conductivity in skutterudites.

## II. GROUND STATES, PHASE STABILITY, AND SYNTHESIS

We explored low-energy ring configurations among all possible ways of arranging Ge, Te, and Sb atoms on sites of the pnicogen rings in $CoSb_{3-m-n}Ge_mTe_n$ using density functional theory (DFT) calculations, guided by the cluster expansion (CE) method.[13] DFT energies were obtained using the Vienna *ab initio* Simulation Package (VASP)[14] within the generalized gradient approximation (GGA) for exchange and correlation and using the projector augmented wave (PAW) method.[15,16] Formation energies were calculated relative to the thermodynamically stable end compounds ($CoGe_2 + Ge$), ($CoTe_2 + Te$), and $CoSb_3$. Calculated formation energies of 340 ternary configurations of Ge, Te, and Sb over the Sb sublattice are plotted in Fig. 1(a), predicting that ternary

 

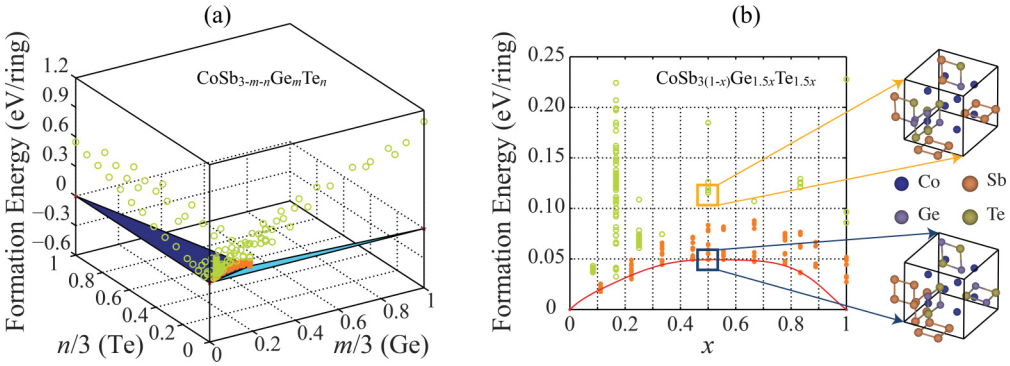


FIG. 1. (Color online) (a) DFT formation energies of all 340 calculated configurations of $CoSb_{3-m-n}Ge_mTe_n$. Configurations featured with CD $Ge_2Te_2$ rings (solid points) have considerably lower energy than those without CD $Ge_2Te_2$ rings (open circles). (b) Formation energies of $CoSb_{3(1-x)}Ge_{1.5x}Te_{1.5x}$. Two typical structures are illustrated at $x = 0.5$. The solid red line is the fifth-order Redlich-Kister polynomial fit to the lower bound of formation energies, which is used to model finite-temperature phase stability.

solid solutions are thermodynamically unstable, with only two skutterudite phases globally stable: $CoSb_3$ and $CoGe_{1.5}Te_{1.5}$ ($R\bar{3}$space-group).[17] Our calculations show that the driving force for phase separation is minimized along the charge-compensated $CoSb_{3(1-x)}Ge_{1.5x}Te_{1.5x}$ tie-line connecting $CoSb_3$ and $CoGe_{1.5}Te_{1.5}$ [$x = 0$ and 1 in Fig. 1(b)]. The lowest energy configurations along the charge-compensated tie-line all contain counter-diagonal (CD) $Ge_2Te_2$ rings, as shown in Fig. 2, visualized using VESTA.[18] As exemplified by the two typical structures in Fig. 1(b), all other ring configurations were found to result in substantially higher formation energies. Figure 2 shows a typical crystal structure with an energetically favorable ring configuration at $x = 0.5$.

Calculated equilibrium lattice parameters of charge-compensated $CoSb_{3(1-x)}Ge_{1.5x}Te_{1.5x}$ exhibit a strong dependence on composition, with an ~11% decrease in volume from $x = 0$ to $x = 1$. The large strain energy penalties accompanying coherent phase coexistence therefore allow charge-compensated solid solutions to form as long as incoherent precipitation is suppressed. Such considerations have proved essential to the understanding of phase stability and high performance in other TE materials, including the well-known lead antimony silver telluride alloy (i.e., $AgPb_mSbTe_{m+2}$).[19,20]

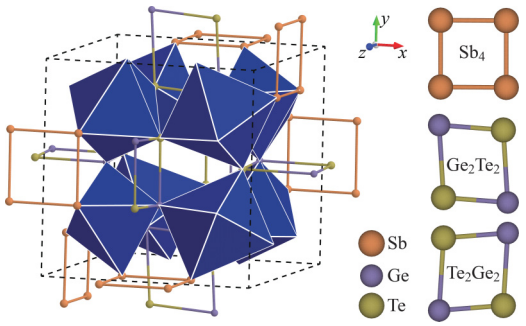


FIG. 2. (Color online) A typical crystal structure (left) of $CoSb_{3(1-x)}Ge_{1.5x}Te_{1.5x}$ at $x = 0.5$, which mixes a variety of rings (right) of $Sb_4$ and CD $Ge_2Te_2$ (or $Te_2Ge_2$). The cubic unit cell contains 32 atoms. The tilting of rings gives rise to the formation of corner-shared octahedrons, which create large cages centering at (0, 0, 0) and (1/2, 1/2, 1/2).

Our DFT energy calculations for $CoSb_{3(1-x)}Ge_{1.5x}Te_{1.5x}$ indicate that it can be approximated as the pseudobinary substitutional alloy $Co_{4/3}[Sb_4]_{(1-x)}[Ge_2Te_2]_x$, where $x$ measures the fraction of $Sb_4$ pnicogen rings that have been substituted with CD $Ge_2Te_2$ rings. Under this constraint, we constructed a free-energy model

$$g(x) = h(x) - Ts(x), \tag{1}$$

per pnicogen ring site, where $h(x)$ is the enthalpy and $s(x)$ is the entropy. The enthalpy was modeled by fitting a fifth-order Redlich-Kister polynomial to the lower bound of DFT formation energies at 0 K, resulting in an expression of the form

$$h(x) = x(1-x)\sum_{n=0}^{5} L_n(1-2x)^n, \tag{2}$$

where the $L_n$ are fitting parameters. The resulting enthalpy model is depicted alongside the first-principles formation energies in Fig. 1(b). The entropy was calculated for an ideal solution of non-interacting $Sb_4$ and CD $Ge_2Te_2$ rings, accounting for the two degenerate orientations of a CD $Ge_2Te_2$ ring, depicted in Fig. 2. The entropy term per ring-site is then

$$\begin{aligned} s(x) = \frac{S}{N} &= \frac{1}{N}k_B \ln\left\{\frac{N!}{(Nx)!\,[N(1-x)]!}\cdot 2^{Nx}\right\} \\ &\approx -k_B\left[x\ln\left(\frac{x}{2}\right) + (1-x)\ln(1-x)\right], \end{aligned} \tag{3}$$

where the second expression is obtained for large $N$ from Stirling's approximation. The resulting total free energy model is

$$\begin{aligned} g(x) = x(1-x)\sum_{n=0}^{5} L_n(1-2x)^n + k_BT\left[x\ln\left(\frac{x}{2}\right)\right. \\ \left. + (1-x)\ln(1-x)\right]. \end{aligned} \tag{4}$$

Minimization of Eq. (4) allowing for the possibility of two-phase coexistence yields the temperature composition phase diagram of Fig. 3(a) (black solid lines). The calculated phase diagram shows a miscibility gap below 600 K between $CoSb_3$ and $CoGe_{1.5}Te_{1.5}$ (which we respectively denote phase $\alpha$ and

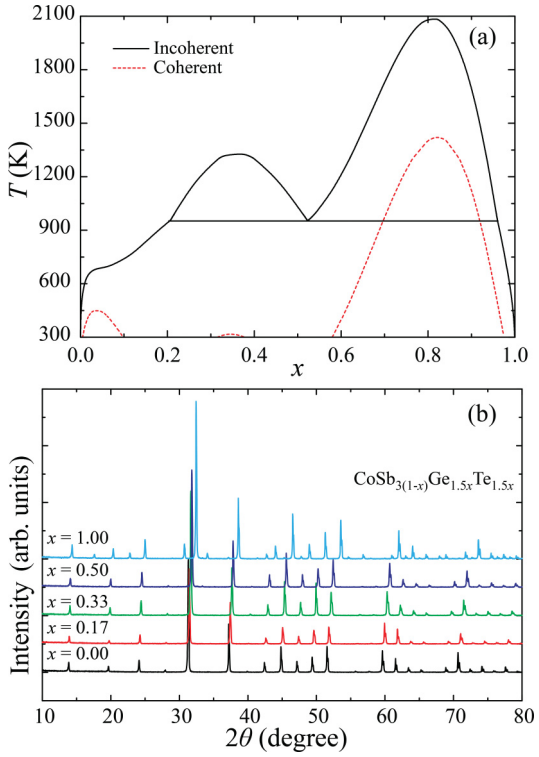


FIG. 3. (Color online) (a) The phase diagram of $CoSb_{3(1-x)}Ge_{1.5x}Te_{1.5x}$. The miscibility gap without coherency strain (solid, black) becomes significantly suppressed by the presence of coherency strain (dashed, red). (b) XRD pattern of various $CoSb_{3(1-x)}Ge_{1.5x}Te_{1.5x}$ samples.

phase $\beta$). Any intermediate composition should result in a coexistence of the $\alpha$ phase and the $\beta$ phase in thermodynamic equilibrium.

The calculated phase diagram of Fig. 3(a) (black lines) describes an incoherent two-phase equilibrium. However, two-phase coexistence can also occur coherently whereby the continuity of crystal planes across the interface between the coexisting phases requires the phase with the larger lattice parameter to be compressed and the phase with the smaller lattice parameter to be stretched. An analysis of phase stability then requires an explicit treatment of the strain energy arising from coherent two-phase coexistence. In general, the strain energy due to coherent two-phase coexistence depends on the microstructure. One possible microstructure is as alternating layers of phase $\alpha$ and phase $\beta$ along a single crystallographic direction. Under additional simplifying assumptions (i.e., concentration independent elastic moduli and a lattice parameter variation with concentration that satisfies Vegard's law), the analysis of coherent two-phase equilibrium becomes straightforward and reduces to the application of a common tangent construction of strain modified homogeneous free energy.[21–23]

Figure 3(a) also shows a phase diagram for coherent two-phase coexistence in $CoSb_{3(1-x)}Ge_{1.5x}Te_{1.5x}$, calculated using the free energy expression Eq. (4) and assuming (i) that the elastic constants are independent of the CD $Ge_2Te_2$ ring concentration (they were taken to be the average of each $c_{ij}$ for $CoSb_3$ and $CoGe_{1.5}Te_{1.5}$, as listed in Table I), and (ii) that the lattice parameters obey Vegard's law. We found that the coherent phase diagram had a negligible dependence on the direction of two-phase separation and on whether plane strain or plane stress constraints in the plane perpendicular to two phase coexistence was used in the energy expression for the elastic strain energy.

As is clear in Fig. 3(a), the miscibility gap is substantially suppressed by the strain energy penalty that emerges if phase separation occurs coherently. In the temperature range relevant to TE applications, this leads to a potentially large solid solution domain for Sb-rich and intermediate compositions (if incoherent precipitation can be suppressed). Coherent phase separation at Ge-Te-rich composition is still predicted to occur, however, in the temperature range of interest.

Following the predicted phase diagram, skutterudite compounds were synthesized using high purity Sb (6N), Co (4N), Te (6N), and Ge (4N) starting materials. Stoichiometric amounts of constituents were weighed in a glovebox under high-purity Ar to prepare $CoSb_{3(1-x)}Ge_{1.5x}Te_{1.5x}$ with $x = 0$, 0.17, 0.33, 0.50, and 1. The charge was sealed in a carbon-coated silica tube under the pressure of $10^{-3}$ Pa and then melted and kept at 1373 K for 30 hours. Subsequently, the ampoules with the melt were quenched in a supersaturated salt water bath, and ingots were annealed at 873 K for 7 days. The obtained material was ground into fine powder in a glovebox and sintered by SPS at 923 K (for $x = 0, 0.17, 1$) and 903 K (for $x = 0.33, 0.50$) for 5 min under the pressure of 40 MPa. X-ray diffraction (XRD) patterns ($2\theta$ 10°–80°) for all samples were collected using a Rigaku Ultima IV X-Ray Diffractometer with Cu K$\alpha$ radiation on powders obtained by grinding the SPS bulks. The experimental XRD patterns, as shown in Fig. 3(b), confirm the existence of a solid solution. A transmission electron microscopy (TEM, JEOL 2010) study showed no Ge-Te-rich nanodots, whose formation we ascribe to the rather more complicated thermodynamics of the imbalanced Ge/Te alloy.

TABLE I. Calculated properties of $CoSb_3$ and $CoGe_{1.5}Te_{1.5}$. The literature results for $CoSb_3$ are also listed. $T_D$, $\gamma_G$, $B$, $c_{ij}$, and $c_v$ are the Debye temperature, the Grüneisen parameter, bulk modulus, elastic constant, and specific heat capacity.

| | $T_D$ (K) | $\gamma_G$ | $B$ (GPa) | $c_{11}$ (GPa) | $c_{12}$ (GPa) | $c_{44}$ (GPa) | $c_v$ (J/mol-K) |
|---|---|---|---|---|---|---|---|
| $CoSb_3$ | 305.9 | 1.11 | 91.89 | 174.6 | 50.52 | 66.34 | 22.9 |
| $CoGe_{1.5}Te_{1.5}$ | 283.5 | 1.28 | 55.87 | 125.6 | 20.40 | 29.35 | 22.9 |
| $CoSb_3$ | 307[a,b] | 0.95[a] | 82[c] | 158[c] | – | 57[c] | – |

[a]From Ref. 25.
[b]From Ref. 26.
[c]From Ref. 27.

### III. LATTICE DYNAMICS AND PHONON CONDUCTIVITY

Because our calculations predict pronounced short-range order of Ge and Te substituted on the pnicogen sublattice and the calculated phase diagram of our model system indicates that a range of compositions exhibiting such short-range order is accessible, we have focused our investigation of heat transport mechanisms on the charge-balanced $CoSb_{3(1-x)}Ge_{1.5x}Te_{1.5x}$ alloy. VASP and PHONON[24] codes were used for the *ab initio* phonon calculations. The total energy and Hellmann-Feynman (HF) forces were found starting from the fully relaxed configuration, such that initial ionic forces were less than $10^{-5}$ eV/Å. Ionic displacements of 0.03 Å of each atom were sampled along the $x$-, $y$-, and $z$-directions. All phonon and thermodynamic properties (Table I, with literature results for $CoSb_3$ also listed[25–27]) are predicted using a fit of interatomic force constant tensors to the calculated HF forces. Diagonalization of the dynamical matrix yields the phonon dispersion, from which density of states and atomic displacement tensors are obtained. The trace of the diagonalized atomic displacement tensor is the atomic displacement parameter (ADP), a scalar measure of single-atom vibration amplitude based on finite-temperature phonon mode occupancy.

ADP values of various low-energy configurations of $CoSb_{3(1-x)}Ge_{1.5x}Te_{1.5x}$ containing CD $Ge_2Te_2$ rings ($x = 0.25$, 0.5, and 1) are shown in Fig. 4(a). Due to the strong covalent bonds of the rings, the ADPs of substitutional atoms are not expected to be large. Surprisingly, the calculated ADP of Ge is significantly larger than that of Sb for all three low-energy configurations considered at $x = 0.25$ and 0.5. For comparison, Fig. 4(a) shows values for the Ba-filled skutterudite $Ba_yCo_4Sb_{12}$ at several values of $y$. The large ADP of the Ba filler atom, relative to most atoms on the pnicogen rings, indicates the rattling behavior of Ba. The rattling behavior of the Ba filler species is believed to cause a reduction in the lattice thermal conductivity of partially filled skutterudites.[28–30]

While the Ge ADP is large for all compositions, it is maximized at $x = 0.5$ where it becomes comparable to that of a Ba filler atom. This suggests that Ge atoms on the CD $Ge_2Te_2$ ring could play a similar role as a rattler. As reported in Refs. 30–32, rattler species inhibit heat transport by both (i) reducing average vibrational frequencies via local bond softening, and (ii) giving rise to low-frequency "guest" vibrational modes decoupled from the host crystal. In addition to having a large ADP, Ge exhibits similar projected phonon dispersion curves to those of Ba, as shown in Fig. 4(b). Phonon modes arising predominantly from either Ba or Ge displacements show negligible dispersion, characteristic of local deformational modes with low group velocity. Note that full band structures and phonon density of states ($D_p$) of various $CoSb_{3(1-x)}Ge_{1.5x}Te_{1.5x}$ compounds are shown in Fig. 5. In spite of this similarity to Ba filler, the collective modes of substituted Ge deform different segments of the skutterudite crystal structure and have different modal frequencies [i.e., Fig. 4(b) for Ge and Ba show 2.27 and 1.52 THz at Γ; 1.24 and 1.45 THz at $X$]. Additionally, the dominant vibrational distortions of Ge responsible for its large ADP are along the diagonal of the CD $Ge_2Te_2$ rings, as illustrated in Fig. 4(c). Collectively, this corresponds to a breathing mode (i.e., expansion/shrinkage) of the cage [Fig. 4(b)]. We consider whether the distinct highly displaced Ge modes and rattler modes of Ba can influence the phonon transport by simultaneously affecting different portions of the phonon spectrum. Our preliminary *ab initio* calculations, as shown in Fig. 5(d), show this hybrid skutterudite structure ($x = 0.5$ and $y = 0.5$, which is close to the filling limit[33]), will retain these distinct features. In particular, our results indicate mode flattening in specific direction (Ge at $X$; Ba at Γ), overall phonon downshift (Ba), and distinct softening induced in the guest vibrational mode frequencies.

Experimental measurements[34] on charge-balanced $CoSb_{3(1-x)}Ge_{1.5x}Te_{1.5x}$ solid solutions show a dramatic decrease in the thermal conductivity with increasing $x$, as

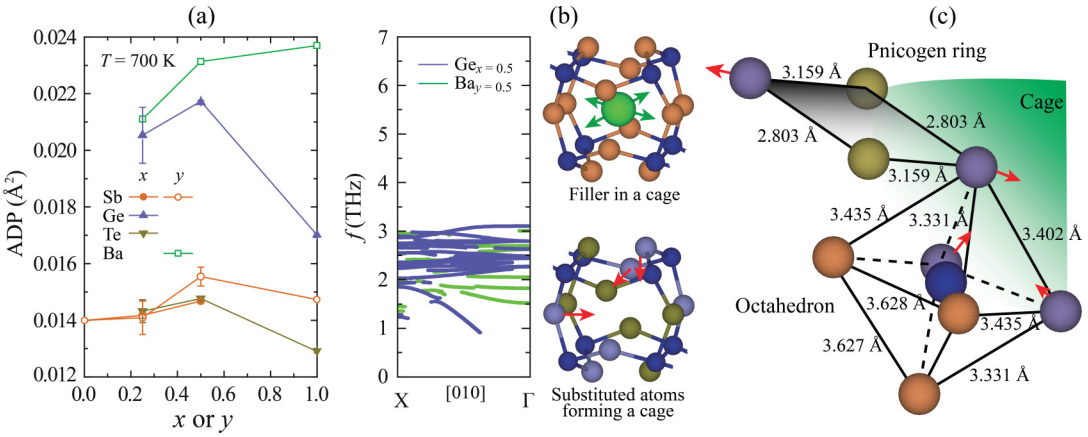


FIG. 4. (Color online) (a) Composition dependence of the mean square displacement for individual atoms (ADP) in atomic-substituted $CoSb_{3(1-x)}Ge_{1.5x}Te_{1.5x}$ and filled $Ba_yCo_4Sb_{12}$. (b) Projected phonon dispersion curves for $x = 0.5$ and $y = 0.5$ using DFT. Atomistic configurations of each vibration mode for filler and double substitution are also given. Blue sphere represents the Co atom. Green sphere represents the Ba filler atom. (c) Atomistic configurations showing a pnicogen ring and octahedron consisting of substituted atoms ($x = 0.5$). Red arrows show the large displacement of each Ge atom.

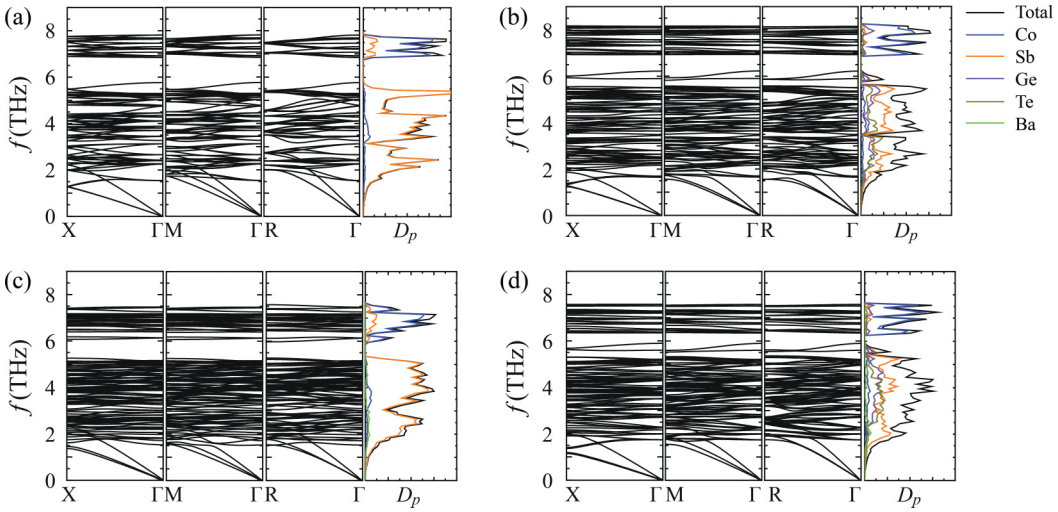


FIG. 5. (Color online) Calculated phonon dispersion curves and density of states: (a) $x = 0$, (b) 0.5, (c) $y = 0.5$, and (d) a hybrid-filled substituted structure ($x = 0.5$ and $y = 0.5$). The site-projected density of states are also shown.

shown in Fig. 6(a). In fact, the minimum in the measured $\kappa_L$ near $x = 0.5$ coincides with the maximum of the calculated Ge ADP. The total measured thermal conductivity can be decomposed as $\kappa = \kappa_L + \kappa_e$, where $\kappa_L$ and $\kappa_e$ are the lattice and electronic thermal conductivity, respectively. An experimental value of $\kappa_L$ is calculated by approximating and subtracting $\kappa_e$, which, in turn, is determined from the Wiedemann-Franz law. Here $\kappa_e = L\sigma_e T$, where $\sigma_e$ is the measured electrical conductivity and $L$ is the Lorenz number,

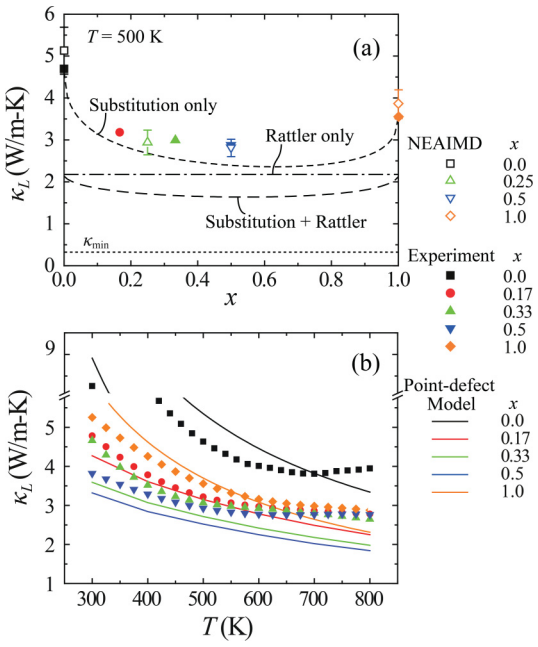


FIG. 6. (Color online) Variations of the predicted lattice thermal conductivity of $CoSb_{3(1-x)}Ge_{1.5x}Te_{1.5x}$, (a) concentration dependence at $T = 500$ K, and (b) temperature dependence for several compositions. Our experimental results (using the Wiedemann-Franz law) and the results of the point-defect model and NEAIMD are shown. The minimum conductivity $\kappa_{min}$ (~0.37 W/m-K) for the amorphous $CoSb_3$ phase[40] is also shown.

determined from the experimental Seebeck coefficient by assuming a single parabolic band.[35] The experimental value of $\kappa_L$ obtained in this way, which Fig. 6(a) shows for several compositions at 500 K, quickly decreases with initial substitution before reaching a plateau at intermediate composition. The temperature dependence of $\kappa_L$, shown in Fig. 6(b), exhibits a decreasing trend at all compositions.

In order to analyze the effect of pnicogen ring substitution on $\kappa_L$, we use experimentally and DFT-parameterized analytical models for phonon-phonon and point-defect scattering,[26,36–40] as well as nonequilibrium *ab initio* molecular dynamics (NEAIMD) simulation.[41]

Starting with $\kappa_L$ of $CoSb_3$ and $CoGe_{1.5}Te_{1.5}$, which are dominated by phonon-phonon scattering, we add an analytical factor for point-defect scattering at intermediate alloy compositions.[37–40,42] Using the Matthiessen rule,[42] the overall $\kappa_L$ with the inclusion of the point-defect scattering is $1/\kappa_L(x,T) = x/\kappa_L(0,T) + (1-x)/\kappa_L(1,T) + 1/\kappa_{L,d}$.[40,43] Here $\kappa_L(0,T)$ and $\kappa_L(1,T)$ are obtained from the Slack relation,[42]

$$\kappa_L(T) = \frac{3.1 \times 10^4 \langle M \rangle \delta T_{D,\infty}^3}{T \langle \gamma_G^2 \rangle N_c^{2/3}}, \tag{5}$$

where $\langle M \rangle$ is the mean atomic weight in the primitive cell, $N_c$ is the number of atoms in a primitive cell, $\delta^3$ is the average volume per atom, $T_{D,\infty}$ is the Debye temperature and $\gamma_G$ is the Grüneisen parameter. For the $\kappa_{L,d}$, the point-defect scattering parameter $\Gamma_s$, including mass fluctuation and atomic displacement,[38,44–46] is

$$\Gamma_s = x(1-x)\left[\left(\frac{\Delta M}{M}\right)^2 + 3\gamma_G^2\left(\frac{\Delta R}{R}\right)^2\right], \tag{6}$$

where $M$ is the average atomic mass of the $CoSb_{3(1-x)}Ge_{1.5x}Te_{1.5x}$ alloy, $R$ is the average atomic radius, and $\gamma_G$ is the Grüneisen parameter. The lattice thermal conductivity limited by the point defect scattering $\kappa_{L,d}$ is

$$\kappa_{L,d} = \frac{k_B}{4\pi u_{p,g,A}(a_1 CT)^{1/2}}, \tag{7}$$

where $CT$ is the relaxation time for phonon-phonon scattering including normal, N-processes, and U-processes. Here $CT$ can be estimated from the experimentally-determined $\kappa_L(0, \mathrm{RT})$ of 8.3 W/m-K for $CoSb_3$. Using

$$CT = \frac{(6n)^{1/3} k_B}{2\pi^{4/3} \kappa_L(0)}, \tag{8}$$

where $n$ is the atomic number density, yields $CT = 4.758 \times 10^{-16}$ s.[40] The parameter $a_1$ is the coefficient for the Rayleigh point-defect scattering rate, given by

$$a_1 = \frac{V_c \Gamma_s}{4\pi u_{p,g,A}^3}, \tag{9}$$

where $V_c$ is the unit cell volume. To clarify this effect with a rattler, the analytical results for the partially filled ($y = 0.5$) and for the hybrid structure (various $x$ with $y = 0.5$) are also shown in Fig. 6(a). Here the overall $\kappa_L$ is given as $1/\kappa_{L,y=0.5}(x,T) = x/\kappa_{L,y=0.5}(0,T) + (1-x)/\kappa_{L,y=0.5}(1,T) + 1/\kappa_{L,d}$,[40,43] assuming $\kappa_{L,y=0.5}(0,T)$ is equal to $\kappa_{L,y=0.5}(1,T)$. Here, $\kappa_{L,y=0.5}(0,T)$ is obtained from the classical MD results in Ref. 40. Using this combined strategy, we predict a further 33% reduction in $\kappa_L$ (much closer to the theoretical minimum, $\kappa_{\min}$, of an amorphous phase).

The lattice thermal conductivity using NEAIMD is computed as the ratio of an applied heat flux to the resulting temperature gradient,

$$\kappa_L = -\frac{\langle q(t) \rangle}{\langle \mathrm{d}T/\mathrm{d}z \rangle}, \tag{10}$$

where the brackets indicate time averages and $q(t)$ is the heat flux. The heat flux is imposed by dividing the simulation cell into sections of equal width, and exchanging kinetic energy between hot and cold sections. The temperature gradient along the $z$ axis is computed from the mean temperature of adjacent sections. For simulations we use the VASP code modified to perform NEAIMD-energy exchange,[47,48] as reported in Ref. 41. The simulations are performed on supercells of 192 atoms ($3 \times 1 \times 2$) and 384 atoms ($6 \times 1 \times 2$), constructed as a solid-solution of pnicogen rings, based on the phase diagram of Fig. 3(a). We equilibrate each simulation using equilibrium AIMD for 1 ps with a 0.5-fs time step. Equilibration is followed by 22 ps of NEAIMD using a 1-fs time step. This duration proved sufficiently long to obtain converged lattice thermal conductivity. Because the exchange of kinetic energy results in non-Newtonian dynamics in the hot and cold sections, only the linear portion of the temperature gradient is considered in calculating the lattice thermal conductivity.

The juxtaposition of the point-defect scattering model and our experimental measurements in Figs. 6(a) and 6(b) indicates favorable agreement between the two, suggesting that the reduction in $\kappa_L$ at intermediate substitution composition can largely be attributed to scattering from point-defects, which take the form of mass disorder and local atomic relaxations. Our analytical model does not account for the effect of bipolar carrier transport in our calculation of $\kappa_e$, likely resulting in overestimation of experimental $\kappa_L$ values at high temperature. As shown in Figs. 6(a) and 6(b), the NEAIMD prediction agrees with experimental and analytical results.

## IV. CONCLUSION

We have demonstrated that Ge/Te double substitution on pnicogen rings is an effective means of lowering the lattice thermal conductivity of skutterudites. Although comparable in magnitude to the effect of Ba filling, Ge/Te substitution targets vibrational modes that are qualitatively different from those of Ba fillers. We therefore expect that a combination of filling and substitutional double doping is likely to act in a complementary manner in suppressing thermal conductivity. This combined strategy should therefore lead to even lower total skutterudite thermal conductivity and higher $ZT$ values than have been realized using either strategy in isolation.

## ACKNOWLEDGMENTS

This work is supported by the Center for Solar and Thermal Energy Conversion, an Energy Frontier Research Center funded by the US Department of Energy, Office of Science, Office of Basic Energy Sciences under Award Number DE-SC0000957. The experimental work at WHUT (synthesis of compounds) is partially supported by the Natural Science Foundation of China (Grant No. 51002112) and International Science & Technology Cooperation Program of China (Grant No. 2011DFB60150) along with 111 Project (Grant No. B07040).

*Corresponding author: cuher@umich.edu

[1] G. A. Slack, in *CRC Handbook of Thermoelectrics*, edited by D. M. Rowe (CRC Press, Boca Raton, FL, 1995), Chap. 34.
[2] D. T. Morelli and G. P. Meisner, J. Appl. Phys. **77**, 3777 (1995).
[3] C. Uher, *Recent Trends in Thermoelectric Materials Research I*, Vol. 69 (Academic Press, San Diego, 2001), p. 139.
[4] H. Li, X. F. Tang, Q. J. Zhang, and C. Uher, Appl. Phys. Lett. **94**, 102114 (2009).
[5] X. Shi, J. Yang, J. R. Salvador, M. Chi, J. Y. Cho, H. Wang, S. Bai, J. Yang, W. Zhang, and L. Chen, J. Amer. Chem. Soc. **133**, 7837 (2011).
[6] I. Oftedal, Z. Kristallogr. **A66**, 517 (1928).
[7] J. L. Feldman and D. J. Singh, Phys. Rev. B **53**, 6273 (1996).
[8] I. K. Dimitrov, M. E. Manley, S. M. Shapiro, J. Yang, W. Zhang, L. D. Chen, Q. Jie, G. Ehlers, A. Podlesnyak, J. Camacho, and Q. Li, Phys. Rev. B **82**, 174301 (2010).
[9] X. Y. Li, L. D. Chen, J. F. Fan, W. B. Zhang, T. Kawahara, and T. Hirai, J. Appl. Phys. **98**, 083702 (2005).
[10] W. S. Liu, B. P. Zhang, L. D. Zhao, and J. F. Li, Chem. Mater. **20**, 7526 (2008).
[11] X. Su, H. Li, G. Wang, H. Chi, X. Zhou, X. Tang, Q. Zhang, and C. Uher, Chem. Mater. **23**, 2948 (2011).
[12] X. Su, H. Li, Y. Yan, G. Wang, H. Chi, X. Zhou, X. Tang, Q. Zhang, and C. Uher, Acta Mater. **60**, 3536 (2012).

[13]J. M. Sanchez, F. Ducastelle, and D. Gratias, Physica A **128**, 334 (1984).
[14]G. Kresse and J. Furthmüller, Phys. Rev. B **54**, 11169 (1996).
[15]P. E. Blöchl, Phys. Rev. B **50**, 17953 (1994).
[16]G. Kresse and D. Joubert, Phys. Rev. B **59**, 1758 (1999).
[17]P. Vaqueiro, G. G. Sobany, and A. V. Powell, Dalton Trans. **39**, 1020 (2010).
[18]K. Momma and F. Izumi, J. Appl. Crystallogr. **44**, 1272 (2011).
[19]S. V. Barabash, V. Ozolins, and C. Wolverton, Phys. Rev. Lett. **101**, 155704 (2008).
[20]S. V. Barabash, V. Ozolins, and C. Wolverton, Phys. Rev. B **78**, 214109 (2008).
[21]J. W. Cahn, Acta Metall. **10**, 907 (1962).
[22]P. W. Voorhees and W. C. Johnson, *Solid State Physics*, Vol. 59 (Academic Press, Elsevier, 2004), p. 1.
[23]A. Van der Ven, K. Garikipati, S. Kim, and M. Wagemaker, J. Electrochem. Soc. **156**, A949 (2009).
[24]K. Parlinski, PHONON software package (Cracow, 2008).
[25]T. Caillat, A. Borshchevsky, and J. P. Fleurial, J. Appl. Phys. **80**, 4442 (1996).
[26]G. P. Meisner, D. T. Morelli, S. Hu, J. Yang, and C. Uher, Phys. Rev. Lett. **80**, 3551 (1998).
[27]L. Zhang, G. Rogl, A. Grytsiv, S. Puchegger, J. Koppensteiner, F. Spieckermann, H. Kabelka, M. Reinecker, P. Rogl, W. Schranz, M. Zehetbauer, and M. A. Carpenter, Mater. Sci. Eng. B **170**, 26 (2010).
[28]B. C. Sales, B. C. Chakoumakos, D. Mandrus, and J. W. Sharp, J. Solid State Chem. **146**, 528 (1999).
[29]G. S. Nolas, D. T. Morelli, and T. M. Tritt, Annu. Rev. Mater. Sci. **29**, 89 (1999).
[30]M. M. Koza, M. R. Johnson, R. Viennois, H. Mutka, L. Girard, and D. Ravot, Nat. Mater. **7**, 805 (2008).
[31]J. Dong, O. F. Sankey, G. K. Ramachandran, and P. F. McMillan, J. Appl. Phys. **87**, 7726 (2000).
[32]M. Beekman, R. P. Hermann, A. Mochel, F. Juranyi, and G. S. Nolas, J. Phys.: Condens. Matter **22**, 355401 (2010).
[33]X. Shi, W. Zhang, L. D. Chen, J. Yang, and C. Uher, Acta Mater. **56**, 1733 (2008).
[34]Thermal diffusivity ($\alpha$) of our new samples was obtained by the laser flash method (Anter Flashline 5000), and converted into thermal conductivity ($\kappa$) using $\kappa = \alpha\rho c_p$, where $c_p$ was the specific heat measured in a Netzsch 404 Pegasus apparatus, and density ($\rho$) was calculated from sample dimensions and mass. Uncertainties in the thermal conductivity measurements are estimated to be $\pm 5\%$.
[35]H. J. Goldsmid, *Electronic Refrigeration* (Pion, London, 1986).
[36]P. G. Klemens, Phys. Rev. **119**, 507 (1960).
[37]J. Callaway and H. C. von Baeyer, Phys. Rev. **120**, 1149 (1960).
[38]B. Abeles, Phys. Rev. **131**, 1906 (1963).
[39]G. S. Nolas, J. L. Cohn, and G. A. Slack, Phys. Rev. B **58**, 164 (1998).
[40]H. Kim, M. Kaviany, J. C. Thomas, A. Van der Ven, C. Uher, and B. L. Huang, Phys. Rev. Lett. **105**, 265901 (2010).
[41]S. Stackhouse, L. Stixrude, and B. B. Karki, Phys. Rev. Lett. **104**, 208501 (2010).
[42]M. Kaviany, *Heat Transfer Physics* (Cambridge, New York, 2008).
[43]B. Huang and M. Kaviany, Acta Mater. **58**, 4516 (2010).
[44]E. F. Steigmeier and B. Abeles, Phys. Rev. **136**, A1149 (1964).
[45]M. Murabayashi, J. Nucl. Sci. Technol. **7**, 559 (1970).
[46]R. Berman, *Thermal Conduction in Solids* (Oxford University Press, Oxford, 1979).
[47]F. Muller-Plathe, J. Chem. Phys. **106**, 6082 (1997).
[48]C. Nieto-Draghi and J. B. Avalos, Mol. Phys. **101**, 2303 (2003).